

Designing Variable Stiffness Profiles To Optimize The Physical Human Robot Interface Of Hand Exoskeletons

Rohit John Varghese^{1*}, Gaurav Mukherjee^{2*}, Raymond King³, Sean Keller³, and Ashish D. Deshpande¹

Abstract—The design of comfortable and effective physical human robot interaction (pHRI) interfaces for force transfer is a prominent challenge for coupled human-robot systems. Forces applied by the robot at the fingers create reaction forces on the dorsal surface of the hand, often leading to high pressure concentrations which can cause pain and discomfort. In this paper, the interaction between the pHRI interface and the dorsal surface of the hand is systematically characterized, and a new method for the design of comfortable interfaces is presented. The variability of the stiffness of the hand dorsum is quantified experimentally, and this data is used to minimize the peak pressure exerted on the hand dorsum, by varying the stiffness profile of the pHRI interface. This optimized design is demonstrated to improve the pressure distribution over the hand dorsum where the robot is attached to the hand. Additionally, to enable informed design choices, the effects of varying the stiffness of the pHRI interface on relative displacement between the robot and the hand dorsum are also characterized. This optimization approach to designing pHRI interface can be extended to different limbs, especially when there is a transfer of high moment loads to the human body, provided the appropriate stiffness data is available.

I. INTRODUCTION

The ideal approach to attaching assistive devices to the human body remains unknown. Designs of attachments, such as shoes, backpacks, clothing, and sporting equipment have evolved to match the contours and articulations of the corresponding body part by using tensioning mechanisms and compliant contact surfaces which help mitigate the effects of moments and forces. While prostheses and wearable robots have embraced these design techniques, the areas of contact between the device and the human body still experience injury and degradation of tissue health. The current approach to designing the contact surfaces, such as sockets for prostheses, is labor intensive, and a quantified approach to generating optimal physical human robot interaction (pHRI) interface designs for high load applications is lacking.

While prosthetic and exoskeletal technology has been improving greatly, rate of disuse of assistive devices remains

*These two authors contributed equally

¹R. J. Varghese and A. D. Deshpande are with the Department of Mechanical Engineering, University of Texas at Austin, Austin, Texas 78712, USA (email: rohitjohnv@utexas.edu, ashish@austin.utexas.edu)

²G. Mukherjee is with the Department of Mechanical Engineering, University of Washington, Seattle, WA 98195, USA (email: mgaurav@uw.edu)

³R. J. King and S. Keller are with Oculus & Facebook, Redmond, WA 98052, USA (email: {raymond.king, sean.keller}@oculus.com)

high [1] [2]. One crucial cause of this is discomfort due to a mismatch of the stiffness between the human limb and the pHRI interface. Designs of pHRI interfaces with uniform stiffness result in localized pressure over bony prominences, and are therefore not ideal [3]. The discomfort due to a uniform pHRI interface is commonly addressed by loosening the straps and reducing the pressure between the pHRI interface and the corresponding contact surface on the human body, also called bias pressure. Reducing the bias pressure to improve comfort between the mismatched surfaces causes relative movement between the robot and the human, which reduces the accuracy of position control [4], causes increased transmission losses [5], and gives rise to inappropriate reaction forces [6], which, ironically, again results in discomfort among users [7]. Discomfort is characterized by high localized pressures [8] [9] which over time lead to the degradation of the tissue structures underneath the points of attachment, resulting in pressure sores [3].

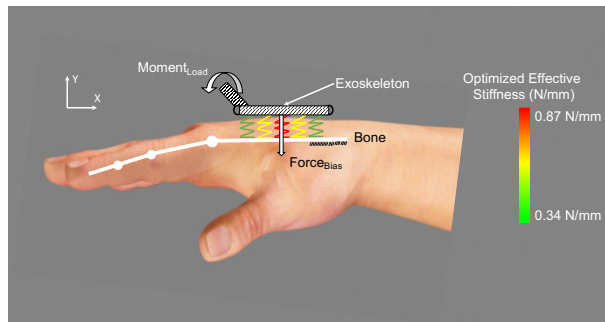


Fig. 1. Diagram of an exoskeleton interface with optimized varying stiffness profile on the dorsum of the human hand. While the traditional approach to attaching devices on the hand does not take into account the ability to vary the stiffness of the pHRI, our method proposes an optimal stiffness profile that minimizes localized pressure concentrations.

Our goal is to improve comfort by minimizing localized loading and by distributing the pressure over the hand dorsum (Fig. 1). Our approach was to measure the spatial stiffness distribution of the hand dorsum, and using these values, to vary the stiffness of the pHRI interface to achieve our goal of minimizing the localized pressures at the contact surface between the pHRI interface and the hand dorsum. While the general idea of stiffness matching has been explored before [7], a systematic design and analysis has not been performed. To apply this approach of impedance or stiffness matching to the hand, additional

constraints must be addressed. Specifically, the contact surface between the hand and hand exoskeletons such as the Maestro [10] and the HX [6] experiences acyclic dynamic forces and moments associated with the high degree of dexterity in hand movements. Therefore an ideal approach to attaching devices to the hand is dependent on multiple criteria, such as the range of external loads applied to the pHRI interface, the stiffness gradient across the surface of the hand and the static pressure that is applied to hold the attachment to the hand under no-loading conditions.

On the Maestro Hand Exoskeleton (Fig. 2), a linkage system is attached between the fingers and the plate strapped to the hand dorsum [11] and consequently, the reaction force and moments of all loads applied to the fingers are borne by the dorsum attachment (the pHRI interface) and the hand. The red straps (Figure 2) apply the pretension required to hold the plate and the linkage to the hand dorsum and the index finger.

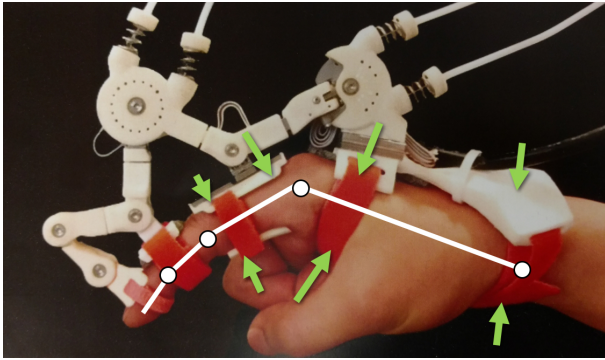


Fig. 2. Maestro Hand Exoskeleton, with force arrows indicating various locations of pHRI interface in this system.

In this paper, we present a novel method to design a pHRI interface that minimizes localized pressures over the hand dorsum. We drive the design of the pHRI interface to achieve this optimality by measuring the stiffness of the hand dorsum, and by systematically varying the effective stiffness of the pHRI interface spatially over the region of contact with the hand. We analyze the behavior of the system using a numerical simulation environment and identify relationships between applied external load, bias force and the optimal stiffness profiles. We demonstrate that creating varying stiffness patterns of the attachment allows us to control the pressure distribution over the dorsum.

The main contribution of this work is a unique optimization based approach to engineering comfortable pHRI interfaces for attaching robotic systems to the human hand dorsum. In addition, we demonstrate the trade-offs that this design approach may have on performance metrics of the coupled human-robot system, such as relative displacement between the robot and the human. We believe that this systematic approach to creating the ideal pHRI interface for

hand exoskeletons can be easily extended to other parts of the human body as well.

II. METHODS

A. pHRI Interface Model

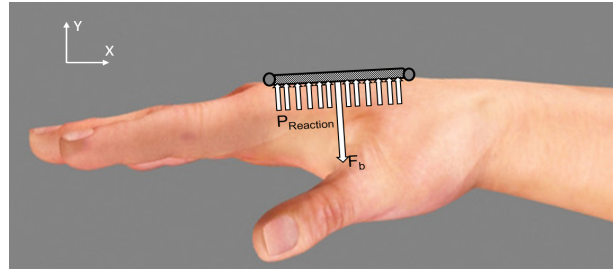


Fig. 3. Hand dorsum and simplified pHRI with uniform stiffness, bias force (F_b), applied using straps and approximated as a point load at the center, and reaction pressure (P_{Reaction}).

We model the pHRI (Fig. 3) as a discrete array of springs representing the hand dorsum (k_{dorsum}) and the pHRI (k_{pHRI}) interface respectively. These two arrays of springs are in series with each other (Fig. 4).

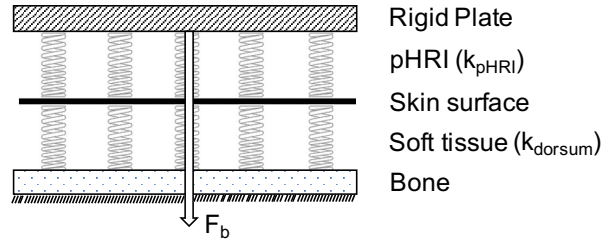


Fig. 4. Modeling all compliant elements between the human reference structure (our skeleton) and the rigid links of the robot. The stiffness of the hand dorsum (k_{dorsum}) and the pHRI (k_{pHRI}) behave as a set of viscoelastic springs in series.

Through analysis of the simplified system under external load, we deduce the shape of the desired effective stiffness (k_{eff}) of this series spring model that allows us to minimize the peak pressures at the contact surface (Section II.B). Using a numerical simulation environment, we compute the optimal effective stiffness gradient which satisfies the deduced shape profile from the analysis, and that also minimizes peak pressure (Section II.C). Next, we quantify the stiffness profile of the experimenter's hand (k_{dorsum}) through an indentation experiment with a robot (Section II.D). The k_{eff} computed from the numerical simulation and k_{dorsum} , obtained experimentally, are then used to compute the stiffness of the pHRI interface (k_{pHRI}). With the resultant optimal pHRI interface stiffness map (Section II.E), we characterize the relationship between four parameters: the bias force (F_b), which is the representation of strap force preloading the pHRI interface to the hand dorsum under no load condition; the relative displacement, which is the shift of the plate of the exoskeleton with respect to the bone; the gradient of stiffness, which is the ratio of difference between

the stiffness at the center and the edge over the stiffness at the center of the pHRI interface ($k_{mid} - k_{edge}/k_{mid}$); and the peak pressure on the hand dorsum, as a result of external loading due to the hand exoskeleton.

B. Analytical determination of optimal stiffness profile for the pHRI interface

To design an optimal pHRI interface for the hand dorsum, (Fig. 1), we simplify the complex interaction at the interface of the hand dorsum and the pHRI interface as two plates of length L and uniform width sandwiched between the rigid reference plate of the Maestro robot, and the rigid human bone. The robot reference plate is held to the dorsum by a bias force mimicking a strap (F_b), applied normally and at $L/2$ (Fig. 5).

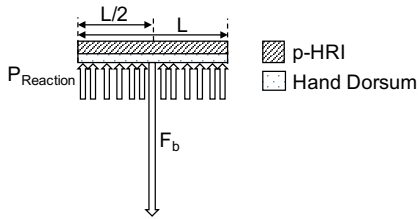


Fig. 5. Model of hand dorsum and pHRI interface with uniform stiffness, bias force (F_b), and uniform reaction pressure ($P_{reaction}$) distribution.

We then load the pHRI interface with an external force mimicking the reaction forces from the Maestro actuators. Using the principle of transmissibility, we express the applied external force to the attachment plate as a combination of an equivalent force and moment applied at the center of the plate, placed coaxially with the bias force. The resulting reaction pressure ($P_{reaction}$) distribution balances the net force (F_b plus the normal component of F_L) and the external moment (M_L) (Fig. 6). Shear loading is considered to be independent and neglected in this section, however, it is considered later in the paper in our overall numerical simulations.

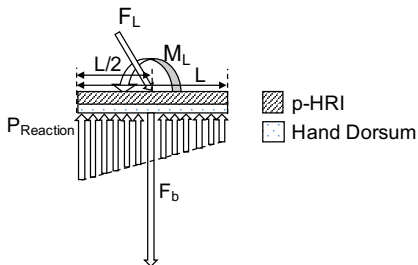


Fig. 6. Model of hand dorsum and pHRI interface with uniform stiffness, bias force (F_b), externally applied force (F_L), moment load (M_L) and reaction pressure ($P_{reaction}$) distribution.

Our objective is to balance the applied force and moment while minimizing peak reaction pressure (C_i) along the contact surface between the two plates.

$$C_i = \max(P_{reaction}) \quad (1)$$

Under the counter-clockwise external moment, M_L , applied on the system, minimizing the cost function, C_i gives us a pressure distribution with two regions of optimized uniform reaction pressure (P_{opt}) below the plate (Fig. 7).

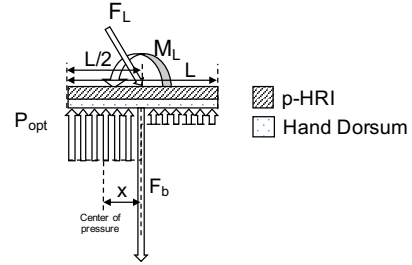


Fig. 7. Model of hand dorsum and pHRI interface with minimized pressure distribution, bias force (F_b), externally applied force (F_L), moment load (M_L) and resulting two regions of optimal reaction pressure (P_{opt}) distribution.

Since we assume that the sum of pressure is equal to the applied load, minimizing the peak pressure would distribute it over a larger area giving us a region of uniform pressure. However, uniform pressure across the entire plate cannot balance the counter-clockwise applied moment, which explains the existence of two sections of different uniform pressure. This orientation of this reaction pressure distribution depends on the direction of the external loading and reverses itself when the external loading is in the clockwise direction.

The boundaries of the regions of uniform pressure shift depending on the ratio of external applied moment (M_L) to the external applied force (F_L). The position of ' x ', the center of the highest pressure region in the optimal distribution (P_{opt}), and P_{peak} , the magnitude of the highest pressure between the two uniform distributions, are computed in (2) and (3).

$$x = \frac{M_L}{F_L + F_b} \quad (2)$$

$$P_{peak} = \frac{F_L + F_b}{L - 2x} \quad (3)$$

The optimal value of bias force, F_b of the attachment against the dorsum, to minimize C_i for the given force and moment loading configuration, is calculated to be the lowest value that gives us a non-negative pressure region (4):

$$F_b = \frac{4M_L}{L} - F_L \quad (4)$$

The profile of optimal effective stiffness that achieves the optimal pressure (P_{opt}), is a hyperbola with high stiffness in the center of the plate which tapers off towards the edge in the direction of the applied moment, M_L . We simplified this

hyperbolic representation to a linear stiffness profile, decreasing from the highest stiffness at the middle of the attachment (k_{mid}), and symmetrically tapering off to a minimum at each edge (k_{edge}). The symmetry allows the resulting profile to be ideal for external moment loads in either direction. To obtain k_{pHRI} , we need to obtain k_{dorsum} in addition to knowing k_{eff} .

C. Numerical computation of the desired stiffness profile

In order to compute the effective spatial stiffness gradient that minimizes peak pressure, as described in section II.A, and to characterize the relationship between the bias force, the gradient of stiffness, relative displacement between the robot and the human, and the peak pressure over the hand dorsum, we used a pHRI interface simulation environment [12] that was developed to model the forces, pressures and displacements at the pHRI interface under the application of external loads.

Within this environment, the human skeleton, and the links of the coupled robot system are represented as rigid bodies. The necessary constraints are implemented by the method of Lagrange multipliers [13], and simulated through time with an ODE45 solver in the MATLAB 2017b (MathWorks Inc., Natick, MA) environment. The viscoelastic properties of human skin and soft tissue, and any compliant elements of the robot are incorporated as non-linear stiffness and damping elements between the constituent rigid components of the system. These elements are discretized or lumped based on the level of complexity that we wish to simulate at any given surface, with high discretization at surfaces of interest and single lumped parameters on peripheral regions. This allows us to simulate the behavior of a system under the application of internal and external loads, and observe trends in behavior of the complex interaction system. This is especially useful in pilot study experimentation such as ours where large population samples of humans cannot be recruited.

For this study, the dorsum surface was discretized into 15 total points, with the pHRI interacting with the underlying human metacarpal through the stiffnesses k_{pHRI} and k_{dorsum} in series at each point. Piece-wise linear values for both stiffness were used, with k_{dorsum} taken from our experimental results. The system was simulated for varying applied force (F_L) and moment loads (M_L) with varying k_{pHRI} profiles to examine the resulting pressure distribution. The relative displacement of the pHRI interface with respect to the underlying bone, due to F_L , was also captured for each stiffness profile, and these results are presented in the next section.

D. Measurement of hand dorsum stiffness

To measure k_{dorsum} , we designed an indentation system comprised of a Phantom Premium 1.5 high force haptic renderer, which has a high positional accuracy of the end effector ($7 * 10^{-6}$ m). This was used along with an ATI

Nano 17 force torque transducer (having a high force torque sensing accuracy of 0.001N) attached at the end of the linkage as an indenter to probe the hand dorsum (Fig. 8).

We selected five points along a line between the metacarpophalangeal joint and the radial styloid process along the 2nd metacarpal bone, the 3rd metacarpal bone, and along a line between the two metacarpal bones, in the inter-metacarpal region. This region was selected to correspond to the area of the attachment plate on the Maestro exoskeleton. Fig. 9 shows the regions selected for indentation.

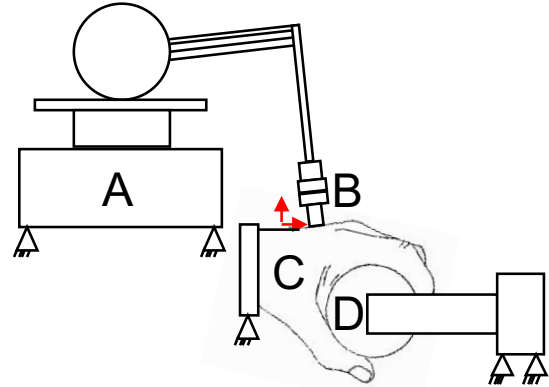


Fig. 8. Phantom premium 1.5 high force haptic renderer (A), instrumented with an ATI nano 17 6-axis force torque transducer (B), probing the hand dorsum (C) over a spatial grid while the subject grasps a spherical object instrumented with an ATI Nano 17 (D).

A spherical object of diameter 3inches (0.077m), embedded with a 6-axis force torque transducer, was provided to mimic a naturalistic spherical power grasp, and to measure grasp force. The object was grasped with minimum force (0N). The spherical power grasp is a major type in grasp taxonomy [14] and is characterized by thumb abduction and movement of all the metacarpal bones and soft tissue structures in the dorsum. This pose provides a stable surface for the indentation measurements. A consistent grasp pattern was used across trials to minimize its influence on stiffness distributions due to the changes in bone locations and muscle recruitment strategy.

The wrist and arm were supported in braces, and the grasp object, and the wrist and arm supports were repositioned to level the hand dorsum in the transverse anatomical plane (Fig. 8). The phantom probe is then manually led once to each point marked on the dorsum for indentation. The probe uses these points as input into an interpolator to compute a spatial trajectory to follow. The phantom is driven in an open-loop position controlled configuration.

Quantifying the stiffness of the indentation system in the direction normal to the hand dorsum demonstrated the need to account for this value in estimating the stiffness of

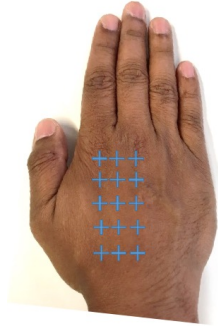


Fig. 9. Locations of measured stiffness measured over the 2nd & 3rd metacarpal, and 2nd-3rd intermetacarpal region. The blue "+" symbols represent the sites of indentation on the hand dorsum

the hand dorsum. The stiffness of the indentation system ($k_{indenter}$) was found to be 2.67 N/mm along the workspace. We account for this stiffness in the measurement of the hand dorsum stiffness (k_{dorsum}) by modeling the interaction between the indentation system and the hand dorsum as two springs in series. The measured stiffness of the hand dorsum, $k_{measured}$, (Fig. 10) is used along with $k_{indenter}$ to calculate the k_{dorsum} (5).

$$k_{dorsum} = \frac{k_{measured} * k_{indenter}}{k_{indenter} - k_{measured}} \quad (5)$$

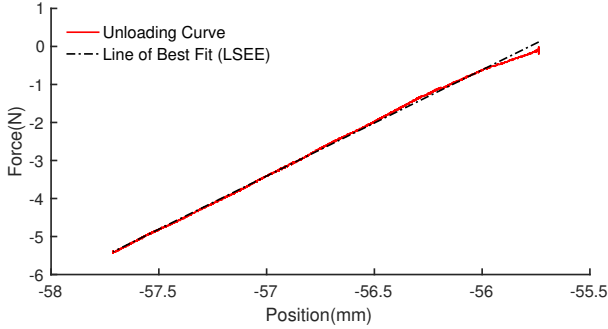


Fig. 10. Fitting a line to the force deflection curve from indentation experiments. The slope of the fitted line corresponds to the measured stiffness.

We made five sequential repeated measures to estimate the variance in the measured stiffness at each point. The observed variance was attributed to movement in the hand. The hand dorsum stiffness data is collected from one pilot subject only, and with a probe having a square base with 4mm edges and 1.5mm fillets on each edge to minimize discomfort during indentation. The indenter profile and size were chosen iteratively based on the relative distribution of the hard and soft tissue structures in the hand. Increasing the resolution of the grid beyond the current levels introduced errors due to partial overlap of soft and hard tissue at the points of measurement.

E. Calculating the optimized padding stiffness

In our model, k_{eff} between the human bone and the Maestro robot's reference plate is comprised of k_{dorsum} and k_{pHRI} in series. Therefore, once we have numerically computed k_{eff} , and measured k_{dorsum} through the indentation experiment, the required k_{pHRI} can be calculated at every point on the attachment surface (6). This gives us a pHRI interface stiffness profile that should generate the minimum peak pressure, or the optimal pressure profile (P_{opt}) on the hand dorsum for the given F_L and M_L .

$$k_{pHRI} = \frac{k_{eff} * k_{dorsum}}{k_{dorsum} - k_{eff}} \quad (6)$$

III. RESULTS

A. Analytical determination of the optimal stiffness distribution

Through an analysis of a simplified two plate model representing the contact between the pHRI interface and the hand dorsum, we found that in order to minimize peak pressures over the hand dorsum, the optimal pressure distribution is comprised of two distinct spatial regions of uniform magnitude (Fig. 7). To achieve this optimal pressure distribution profile, we showed that a linear gradient profile of the effective stiffness, $((k_{mid} - k_{edge})/k_{mid})$ tapering from the center to the edges was a possible solution.

B. Numerical computation of the desired stiffness profile

From the linear gradient profile of the desired effective stiffness described in the analysis (Section III.A), we evaluated the behavior of the entire system, across a range of parameters, with the custom-built numerical simulation environment (Section II.C). Through repeated simulation across the space of applied external moments, bias forces which represent the strap force holding the pHRI interface to the hand dorsum, and stiffness gradient which describes the spatial distribution of the effective stiffness over the pHRI interface, we characterized the effects of these parameters on our primary performance metric, the peak pressure P_{peak} , experienced over the hand dorsum.

From the results of the numerical simulation (Fig. 11), we observed that P_{peak} is minimum at the stiffness gradient of 0.6 for 15N of bias force under M_L of 0.3 Nm. This surface is a visual representation of the sensitivity of P_{peak} , a proxy for user discomfort, to stiffness gradient and the bias force.

C. Hand dorsum stiffness

The stiffness of the hand dorsum was measured and characterized with five repetitions over each of the 15 chosen points, distributed equally over the 2nd metacarpal, 3rd metacarpal and the inter-metacarpal gap between these

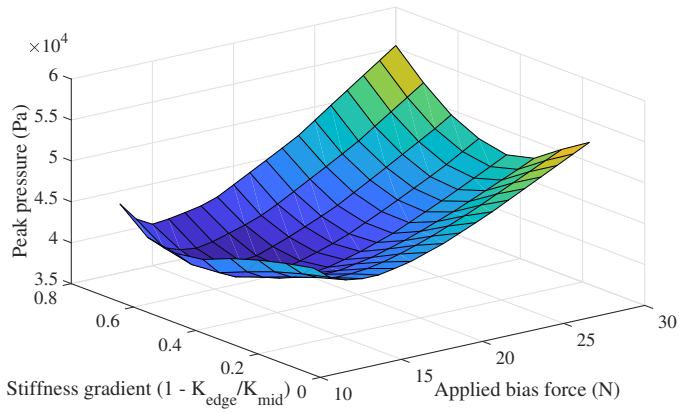


Fig. 11. Effect of varying bias force and stiffness profiles on the peak pressure across the interface. The minimum satisfies the calculated values of optimal bias force in equation 3.

bones on a single subjects hand (Fig. 12). On average, k_{dorsum} was measured to be 1.0876 ± 0.40 N/mm over a range of from 0.54 N/mm to 1.59 N/mm. The region of the dorsum above the metacarpal bones was found to be stiffer (1.1285 ± 0.43 N/mm) than the region between the bones (1.0060 ± 0.36 N/mm) that accommodate soft tissue. Increasing force of grasp led to an increase in measured dorsum stiffness (Fig. 12), however, the pHRI interface stiffness computed here is for a grasp force of 0 N.

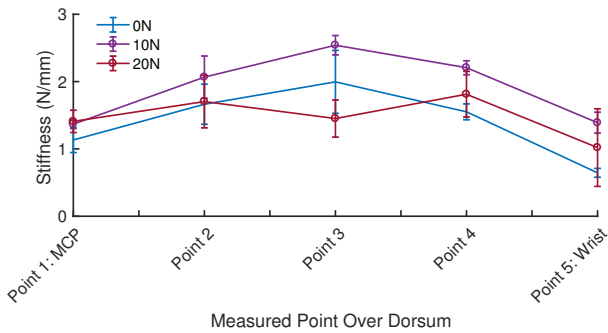


Fig. 12. Measured stiffness of the hand dorsum for five equally spaced points along the second metacarpal at three levels of grasp force applied by the subject.

D. Optimal pHRI interface stiffness

The stiffness of the optimal pHRI interface was computed from the numerically determined k_{eff} and the k_{dorsum} (6), for each point on the hand dorsum (Fig. 13), for a force of grasp of 0N. On average, the k_{pHRI} was found to be 1.6460 ± 1.47 Nm. The pHRI interface over the metacarpal bones was less stiff (1.3478 ± 0.8054 Nm) than the pHRI interface between the bones (2.2424 ± 2.33 Nm), demonstrating that loading the soft tissue to a higher degree minimizes the P_{peak} .

E. Relationship between design parameters

From the numerical simulation outlined previously (Section II.B), we quantify the effects of varying applied

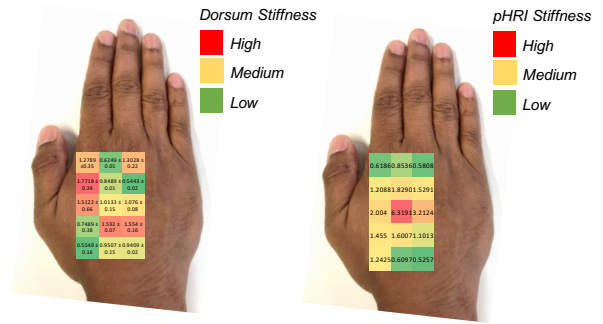


Fig. 13. Heat maps of the measured dorsum stiffness (left) and the calculated optimal pHRI stiffness for each corresponding point (right).

moments, bias forces and stiffness gradients on our primary performance metric of peak pressure experienced at the interface. When compared to a uniform stiffness distribution (stiffness gradient of 0), we observe an improvement in P_{peak} for all cases of M_L when the k_{eff} is varied as a gradient from the center to the edge. With increasing M_L , we observe the percentage improvement to become more pronounced (Fig. 14). Additionally, the optimal value of stiffness profile gradient is dependent on M_L , and is seen to increase linearly with the ratio (M_L/F_L).

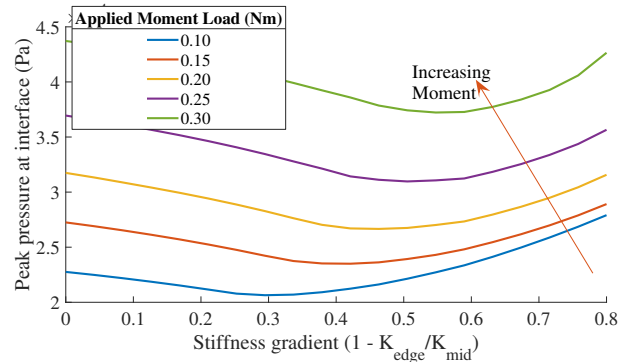


Fig. 14. Plot of peak pressure on the interface surface for varying stiffness profile gradients, at each value of applied moment load, with the applied bias force held constant.

The simulation confirms the expected outcome that the highest values of P_{peak} are observed at the highest M_L for all conditions of the k_{eff} . Therefore, the optimal stiffness profile is tuned for the highest M_L that the specific device will experience. With this condition, we can observe a 15% improvement in P_{peak} experienced by using a stiffness profile gradient of 0.6 from the center to the edges of the attachment, for the highest M_L of 0.3Nm. These loading conditions are derived from the Maestro exoskeleton.

While minimizing user discomfort is critical, other performance metrics including the relative displacement across the pHRI interface can also be examined with this approach. When considering the effect of these same input variables of bias force and stiffness gradient on the

relative displacement, it becomes evident that we have a trade-off between our performance metrics of comfort and relative displacement. Fig. 15 shows the effect on relative displacement due to a change in stiffness profiles with the applied force and moment loading held constant. Contrary to the effect on peak pressure shown earlier, the relative displacement increases with the stiffness profile gradient.

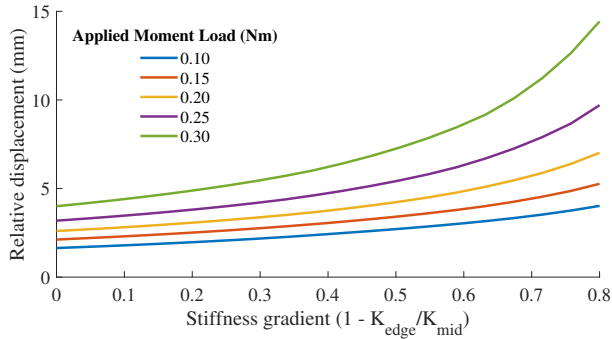


Fig. 15. Plot of the effect on relative displacement between the robot reference and the human skeleton on changing the stiffness profile gradient of the pHRI. Each line represents the effect due to a change in the pHRI stiffness gradient while holding the applied moment constant.

This is more clearly illustrated in Fig. 16, where the two output metrics are plotted against the stiffness profile gradient on identical x-axes. It shows that increasing the stiffness profile gradient to improve the peak pressure across the interface has an adverse effect on the relative displacement.

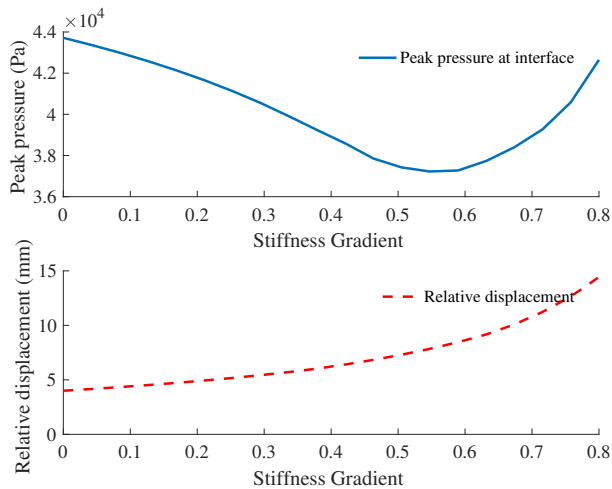


Fig. 16. Trade-off between peak pressure (as a measure of user comfort) and relative displacement on varying the stiffness profile gradient.

We also observe a similar trade-off between peak pressure at the interface and relative displacement while varying bias force (Fig. 17).

IV. DISCUSSION

Our analysis of the force distribution at the pHRI interface showed that under force and moment loading, the

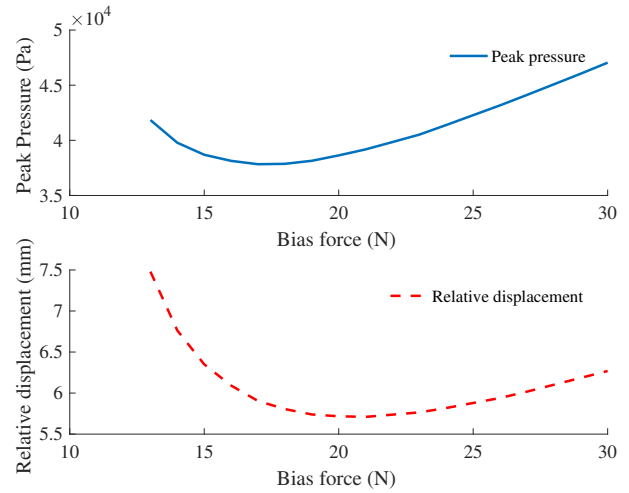


Fig. 17. Trade-off between peak pressure and relative displacement on varying the bias force applied.

performance metric of peak pressure at the contact surface can be minimized by using a spatially varying stiffness distribution of the pHRI interface. A solution that gives us this optimal force distribution was shown to be a linearly decreasing stiffness gradient from the center to the edges of the pHRI interface.

The performance of the effective stiffness gradient was numerically quantified using a MATLAB based simulation engine. By simulating a range of applied bias force and stiffness gradients, we are able to show a minimum in the peak pressure as predicted by our analytical model. This optimal stiffness gradient showed a 15% reduction in peak pressure over the hand dorsum when compared with uniform stiffness, under external loading of 0.3Nm. It should be noted though, that the value of optimal stiffness gradient between the human and the exoskeleton is dependent on the applied moment, M_L . Since the largest peak pressures experienced by this system are always under the conditions of highest applied moment loading, we must therefore consider the highest moment that our system is likely to experience when computing the k_{eff} .

The optimal effective stiffness gradient described above denotes the effective stiffness of the pHRI interface and the soft tissue on the human dorsum acting in series. Therefore, in order to design the pHRI interface to a desired stiffness profile, the knowledge of the dorsum stiffness is an important parameter to quantify. Our pilot experimental study characterized the spatial range and distribution of dorsum stiffness on a single hand. The measured stiffness values at the MCP joint are lower than originally anticipated, which could potentially be due to the soft extensor tendon hood over this region. The measured dorsum stiffness data provides us with initial values necessary for pHRI interface design methods presented here. Systematically characterizing the dorsum stiffness across the hand pose and

grasp force for multiple subjects will help further clarify the underlying relationships dictating optimal pHRI design that we have demonstrated here, for the first time.

With numerical values available for both the desired effective stiffness distribution and the measured dorsum stiffness, we are able to inform the design of the pHRI interface stiffness. This is the only stiffness property available to controllably design, as the properties of the human tissue cannot be changed. Since the optimal effective stiffness (between the human bone and the robot reference) is the series equivalent of the pHRI interface stiffness and the stiffness of the human dorsum, the optimal pHRI stiffness is calculated from the knowledge of both the optimal effective stiffness and the measured dorsum stiffness. This is why the characterization of both is essential to this method. A generalizable takeaway from this study is that a pHRI interface designed to reduce P_{peak} exerted under moment loading must have regions of low k_{eff} towards the edges. In design, this region of low stiffness can be achieved by using more compliant padding near the edges.

The design changes presented can potentially help reduce user discomfort by reducing the peak pressure applied on the human at the contact surface. However, we showed that these same changes can adversely affect another performance metric of coupled human-robot systems: the relative displacement of the attachment with respect to the human skeleton. The trade-off between the two performance metrics of user comfort and relative displacement on varying our design inputs of stiffness gradients and bias forces will help make informed design choices, driven by the desired requirements of our application.

V. CONCLUSION

The primary contribution of this paper is a new design method for pHRI interfaces that minimizes the peak values of concentrated pressure applied to the hand dorsum by the use of a spatially varying stiffness profile. This method is informed by calculations of the optimal pressure distribution as well as experimental measurement of stiffness of the human hand dorsum. By characterizing the effect of the proposed non-uniform pHRI interface stiffnesses on the relative displacement between the hand and the exoskeleton, we highlight the need to keep relative displacement in mind while optimizing for the minimal peak pressure distribution. This is also the first study, to our knowledge, that leverages the measured biomechanical characteristic of stiffness of the human hand to design an optimal interface stiffness profile.

This study provides a starting point for our ongoing work of in-depth characterization of the interaction between exoskeletons and the human hand. The analytical and simulation results based on performance metrics shown to influence

user comfort provide us with an important direction in designing better pHRI interfaces. Further research involving human subject studies will be important in validating the results presented here and for examining user comfort and sustained use of devices. Further study will also focus on extending the generalizability of the findings in this paper. These methods can be expanded to characterize more complex bias or strap systems, and will be used for proposing further design guidelines for the development of attachment devices in coupled human-robot systems. This novel approach of quantifying body stiffness, and optimizing pHRI interface designs to minimize irregularities in pressure distribution at contact surfaces between humans and exoskeletons can be used to design other wearable devices for the hand, and should be extendable to designs for other limbs.

REFERENCES

- [1] E. Biddiss and T. Chau, "Upper-limb prosthetics: critical factors in device abandonment," *American journal of physical medicine & rehabilitation*, vol. 86, no. 12, pp. 977–987, 2007.
- [2] K. Hagberg, E. Häggström, M. Uden, and R. Brånemark, "Socket versus bone-anchored trans-femoral prostheses: hip range of motion and sitting comfort," *Prosthetics and orthotics international*, vol. 29, no. 2, pp. 153–163, 2005.
- [3] A. J. Petron, "Prosthetic Socket Design: From a Multi-Indenter Device for in vivo Biomechanical Tissue Measurement to a Quasi-passive Transtibial Socket Interface," p. 197, 2016.
- [4] T. Lenzi, N. Vitiello, S. M. M. D. Rossi, A. Persichetti, F. Giovacchini, S. Roccella, F. Vecchi, and M. C. Carrozza, "Measuring human-robot interaction on wearable robots: A distributed approach," *Mechatronics*, vol. 21, no. 6, pp. 1123–1131, 2011.
- [5] M. B. Yandell, B. T. Quinlivan, D. Popov, C. Walsh, and K. E. Zelik, "Physical interface dynamics alter how robotic exosuits augment human movement: implications for optimizing wearable assistive devices," *Journal of NeuroEngineering and Rehabilitation*, vol. 14, no. 1, p. 40, 2017.
- [6] M. Cempini, A. Marzegan, M. Rabuffetti, M. Cortese, and N. Vitiello, "Analysis of relative displacement between the HX wearable robotic exoskeleton and the user's hand," 2014.
- [7] A. Petron, J.-F. Duval, and H. Herr, "Multi-Indenter Device for in vivo Biomechanical Tissue Measurement," *IEEE Transactions on Neural Systems and Rehabilitation Engineering*, vol. 25, no. 5, pp. 1–1, 2016.
- [8] T. A. Krouskop, R. Williams, M. Krebs, I. Herszkowicz, and S. Garber, "Effectiveness of mattress overlays in reducing interface pressures during recumbency," *Journal of rehabilitation research and development*, vol. 22, no. 3, pp. 7–10, jul 1985.
- [9] M. Belda-Lois, J.M.; Poveda, R.; Vivas, *Analysis of Pressure Distribution and Tolerance Areas for Wearable Robots*, 2008.
- [10] Y. Yun, S. Dancusse, P. Esmatloo, A. Serrato, C. A. Merring, P. Agarwal, and A. D. Deshpande, "Maestro: An emg-driven assistive hand exoskeleton for spinal cord injury patients," in *Robotics and Automation (ICRA), 2017 IEEE International Conference on*. IEEE, 2017, pp. 2904–2910.
- [11] P. Agarwal, J. Fox, Y. Yun, M. K. OMalley, and A. D. Deshpande, "An index finger exoskeleton with series elastic actuation for rehabilitation: Design, control and performance characterization," *The International Journal of Robotics Research*, vol. 34, no. 14, pp. 1747–1772, 2015.
- [12] R. J. Varghese, "Physical human-robot interaction (phri) interfaces: A simulation based design method," Master's thesis, The University of Texas at Austin, 2017.
- [13] F. Udwardia and R. E. Kalaba, "What is the General Form of the Explicit Equations of Motion for Constrained Mechanical Systems?" *Journal of Applied Mechanics*, vol. 69, no. 3, p. 335, 2002.
- [14] T. Feix, J. Romero, H. Schmiedmayer, A. Dollar, and D. Kragic, "The grasp taxonomy of human grasp types," *IEEE Transactions on Human-Machine Systems*, 2015.